

PHOTOCATALYTIC REACTION OF HETEROSTRUCTURE $\text{Ag}_{0.9}\text{Pd}_{0.1}/\text{Bi}_2\text{WO}_6$ NANOCOMPOSITES TO RHODAMINE B UNDER VISIBLE LIGHT IRRADIATION

T. BUNLUESAK^a, A. PHURUANGRAT^{a,*}, S. THONGTEM^{b,c},
T. THONGTEM^{c,d}

^a*Department of Materials Science and Technology, Faculty of Science,
Prince of Songkla University, Hat Yai, Songkhla 90112, Thailand*

^b*Department of Physics and Materials Science, Faculty of Science,
Chiang Mai University, Chiang Mai 50200, Thailand*

^c*Materials Science Research Center, Faculty of Science, Chiang Mai University,
Chiang Mai 50200, Thailand*

^d*Department of Chemistry, Faculty of Science, Chiang Mai University,
Chiang Mai 50200, Thailand*

Bi_2WO_6 thin nanoplates were modified by 5% by weight of bimetallic $\text{Ag}_{0.9}\text{Pd}_{0.1}$ nanoparticles to form Schottky barrier by photoreduction method. The as-synthesized heterostructure 5% $\text{Ag}_{0.9}\text{Pd}_{0.1}/\text{Bi}_2\text{WO}_6$ nanocomposites were characterized by X-ray diffraction (XRD), transmission electron microscopy (TEM), X-ray photoelectron spectroscopy (XPS), Fourier Transform Infrared Spectrophotometry (FTIR) and Raman spectroscopy. XRD pattern of heterostructure 5% $\text{Ag}_{0.9}\text{Pd}_{0.1}/\text{Bi}_2\text{WO}_6$ nanocomposites showed only orthorhombic Bi_2WO_6 structure due to the low loading content and small particle size of bimetallic AgPd nanoparticles. TEM image of heterostructure 5% $\text{Ag}_{0.9}\text{Pd}_{0.1}/\text{Bi}_2\text{WO}_6$ nanocomposites shows a number of sphere-like bimetallic AgPd nanoparticles embedded on top of Bi_2WO_6 thin nanoplates. The photocatalytic activities of pure Bi_2WO_6 sample and heterostructure 5% $\text{Ag}_{0.9}\text{Pd}_{0.1}/\text{Bi}_2\text{WO}_6$ nanocomposites were studied through the photodegradation of rhodamine B (RhB) under visible light irradiation. The heterostructure 5% $\text{Ag}_{0.9}\text{Pd}_{0.1}/\text{Bi}_2\text{WO}_6$ nanocomposites show photodegradation of RhB under visible light irradiation higher than pure Bi_2WO_6 nanoplates. The enhanced photocatalytic properties of the heterostructure 5% $\text{Ag}_{0.9}\text{Pd}_{0.1}/\text{Bi}_2\text{WO}_6$ nanocomposites are attributed to the efficient separation of photoinduced carriers at the interface of bimetallic $\text{Ag}_{0.9}\text{Pd}_{0.1}$ nanoparticles and Bi_2WO_6 nanoplates. A possible photocatalytic mechanism is also proposed according the experimental results.

(Received July 15, 2020; Accepted September 10, 2020)

Keywords: AgPd; Bi_2WO_6 ; Nanocomposites; Photocatalysis

1. Introduction

In recent years, semiconductor-based photocatalyst is one of the most promising materials used for environmental purification because it is inexpensive and has high efficiency in transforming organic pollutant molecules into small inorganic molecules [1-3]. TiO_2 as a semiconducting photocatalyst with large band gap of about 3.2 eV has been intensively studied because of its high photoactivity, good photostability, low cost and nontoxicity [1-4]. However, TiO_2 is able to absorb only UV light with the content of less than 5% of sunlight [1-3,]. Thus, novel photocatalyst driven by visible light is increasing much attention in utilizing of visible light of about 46% of solar radiation for the degradation of pollutants in wastewater [1, 3, 4].

* Corresponding author: phuruangrat@hotmail.com

Among various studied photocatalysts, bismuth tungstate (Bi_2WO_6) as n-type semiconductor with narrow band gap of 2.6–2.8 eV is a prominent candidate in degradation of organic compounds in wastewater due to its narrow band gap, good stability, wide solar energy response, no photo-corrosion, high visible absorption and good photocatalytic activity [3, 4, 5-7]. Nevertheless, its photocatalytic application is still limited because of its high recombination rate of photogenerated electron-hole pair and low photo quantum efficiency [3, 5-8]. Introducing noble metal onto semiconductor photocatalyst is an effective method to improve photocatalytic activity by the formation of Schottky barrier at the interface of noble metal and semiconductor photocatalyst, including the effective suppression of photogenerated electron-hole recombination [9-12]. Photogenerated electron transfers from conduction band of semiconducting photocatalyst to noble metal as an electron acceptor and further transforms O_2 to active superoxide radical, which can lead to enhance photocatalytic reaction [9, 11].

In this research, 5% $\text{Ag}_{0.9}\text{Pd}_{0.1}$ nanoparticle-modified Bi_2WO_6 nanoplates were successfully prepared by photoreduction method. The as-prepared $\text{Ag}_{0.9}\text{Pd}_{0.1}$ nanoparticle-modified Bi_2WO_6 nanoplates showed photodegradation of rhodamine B (RhB) under visible light irradiation higher than pure Bi_2WO_6 nanoplates.

2. Experiment

Typically, 0.01 mole of $\text{Bi}(\text{NO}_3)_3 \cdot 5\text{H}_2\text{O}$ and 0.005 mole of Na_2WO_4 were dissolved in 100 ml R.O. water under continued stirring at room temperature to form two clear solutions. The two clear solutions were mixed and adjusted the pH to 6 by 3 M NaOH under continued stirring at room temperature to form a mixture solution containing white precipitates. The whole mixture was put in a 200 ml Teflon-lined stainless steel autoclave, hydrothermally processed at 180 °C in an electric oven for 20 h and cooled down to room temperature. The as-prepared yellow precipitates were separated, washed by water and ethanol several times, and dried at 60 °C for 24 h.

To prepare 5% $\text{Ag}_{0.9}\text{Pd}_{0.1}/\text{Bi}_2\text{WO}_6$ nanocomposites, 4.5% AgNO_3 , 0.5% PdCl_2 by weight and 2.50 g of the as-prepared Bi_2WO_6 nanoplates were put in 100 ml ethylene glycol under continued stirring at room temperature for 30 min and were irradiated by visible light for 1 h under continued stirring. The as-prepared 5% $\text{Ag}_{0.9}\text{Pd}_{0.1}/\text{Bi}_2\text{WO}_6$ nanocomposites were separated, washed by water and ethanol for several times, and dried at 60 °C for 24 h for further characterization.

The crystallinity and crystalline phase of the as-synthesized samples were analyzed by X-ray diffraction (XRD, Philips X'Pert MPD) with Cu K_α radiation as an X-ray source in the range of 20°–60°. The morphological investigation was carried out by a transmission electron microscope (TEM, JEOL JEM-2010) at an acceleration voltage of 200 kV. A Fourier transform infrared (FTIR) spectrometer was carried out through a Bruker Tensor 27 spectrometer at room temperature in the range of 400–4000 cm^{-1} . Raman analysis was operated on a T64000 HORIBA Jobin Yvon Raman spectrophotometer using a 50 mW and 514.5 nm wavelength Ar green laser. X-ray photoelectron spectroscopy (XPS) was carried out using an Axis Ultra DLD | Kratos - Kratos Analytical with a 1486.6 eV monochromated Al K_α radiation as a providing source. All XPS spectra were calibrated with respect to a C 1s electron peak at 285.1 eV.

The photocatalytic reaction was carried out in the solution of 200 mg catalyst dispersed in 200 ml of 1×10^{-5} M RhB solution. Prior to irradiation, the suspension was magnetically stirred in the dark for 30 min to establish an adsorption/desorption equilibrium of the dye and the catalyst. During testing, approximately 5 ml samples were withdrawn every 30 min. The aqueous samples were centrifuged to remove any suspended solid particles. The residual concentration of RhB solutions containing in a microcuvette was measured by a UV-visible spectrophotometer (Perkin-Elmer Lambda 25) at 554 nm using R.O. water as a reference. The degradation efficiency was calculated by the equation given below.

$$\text{Decolorization efficiency (\%)} = \frac{C_o - C_t}{C_o} \times 100 \quad (1)$$

C_o is the initial dye concentration and C_t is the dye concentration after testing for a period of time (t).

3. Results and discussion

Phase and crystallinity of the as-obtained Bi_2WO_6 and 5% $\text{Ag}_{0.9}\text{Pd}_{0.1}/\text{Bi}_2\text{WO}_6$ nanocomposites were characterized by XRD as the results shown in Fig. 1. The pure Bi_2WO_6 sample without bimetallic AgPd can be indexed to the orthorhombic Bi_2WO_6 structure with good agreement to the JCPDS no. 73-1126 [13]. No diffraction peaks of impurities were detected in the pattern. Based on the standard data, the intensity of the (113) peak is approximately five times that of the (200) peak. Nevertheless, the intensity ratio of the (113) peak to the (200) peak of the as-prepared Bi_2WO_6 sample was less than 2.5. The results certified that the as-synthesized Bi_2WO_6 sample has anisotropic growth along the (200) direction [14, 15]. The sharp and strong diffraction peaks of both as-obtained Bi_2WO_6 and 5% $\text{Ag}_{0.9}\text{Pd}_{0.1}/\text{Bi}_2\text{WO}_6$ nanocomposites revealed that the samples were highly crystalline. The diffraction peaks of 5% $\text{Ag}_{0.9}\text{Pd}_{0.1}/\text{Bi}_2\text{WO}_6$ nanocomposites did not shift with respect to those of the as-obtained Bi_2WO_6 although the nanocomposites were loaded by AgPd. Thus, a portion of AgPd did not incorporate into the Bi_2WO_6 lattice. They should be noted that no obvious diffraction peaks of AgPd were detected in the pattern of 5% $\text{Ag}_{0.9}\text{Pd}_{0.1}/\text{Bi}_2\text{WO}_6$ nanocomposites. Possibly, the loaded content of AgPd is too low to be detected, the particles of AgPd are in the nano range, bimetallic AgPd nanoparticles are good dispersive and the dominant peaks of Bi_2WO_6 cover the peaks of AgPd nanoparticles [16].

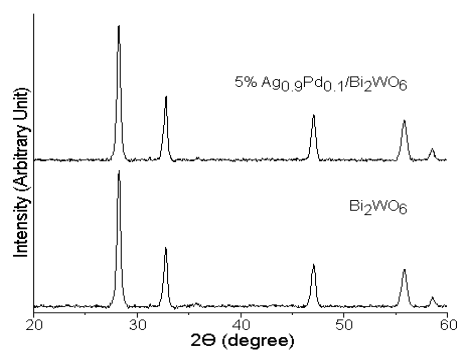


Fig. 1. XRD patterns of Bi_2WO_6 and 5% $\text{Ag}_{0.9}\text{Pd}_{0.1}/\text{Bi}_2\text{WO}_6$ nanocomposites.

Crystal structure of Bi_2WO_6 as Aurivillius-type structure is composed of perovskite-like $(\text{WO}_4)^{2-}$ and fluorite-like $(\text{Bi}_2\text{O}_2)^{2+}$ layers lying normal to the c direction. The WO_6 octahedrons are joined by equatorial oxygen atoms, whereas the apical oxygen atoms join the WO_6 and BiO_6 polyhedrons [14, 17, 18]. Tungsten exhibits a regular octahedral environment and neighbouring octahedrons are connected to each other by corner sharing [14, 17, 18]. Vibration modes in Raman and IR active of Bi_2WO_6 are grouped into six Raman active ($2A_{1g} + B_{1g} + 3E_g$) and nine IR active ($4A_{2u} + 5E_u$) [14, 19, 20]. These modes are indexed to symmetric (A_{1g}) and asymmetric stretching vibration ($A_{2u} + E_u$) of WO_6 octahedron, bending vibration of WO_6 octahedron ($E_g + 2E_u + A_{2u} + B_{2u}$), stretching and bending vibration of the $(\text{Bi}_2\text{O}_2)^{2+}$ layer ($B_{1g} + E_g + A_{2u} + E_u$), translational motion of Bi^{3+} ions ($A_{1g} + E_g$) and vibration involving translational motion of Bi^{3+} and W^{6+} ions ($A_{2u} + E_u$) [14, 19]. Fig. 2a

shows FTIR spectra of the as-synthesized Bi_2WO_6 and 5% $\text{Ag}_{0.9}\text{Pd}_{0.1}/\text{Bi}_2\text{WO}_6$ nanocomposites. They show the main absorption FTIR bands at $400\text{--}1000\text{ cm}^{-1}$ which are related to Bi–O stretching, W–O stretching and W–O–W bridging modes in Bi_2WO_6 lattice [2, 15]. The as-synthesized Bi_2WO_6 and 5% $\text{Ag}_{0.9}\text{Pd}_{0.1}/\text{Bi}_2\text{WO}_6$ nanocomposites show FTIR vibration at 828 and 730 cm^{-1} which are related to the W–O and W–O–W vibration of WO_6 octahedron in Bi_2WO_6 lattice [14, 20]. The FTIR peaks at 572 and 445 cm^{-1} of both as-synthesized Bi_2WO_6 and 5% $\text{Ag}_{0.9}\text{Pd}_{0.1}/\text{Bi}_2\text{WO}_6$ nanocomposites were identified to the Bi–O vibration of BiO_6 octahedron in Bi_2WO_6 lattice [21, 22]. The broad FTIR bands located at $3200\text{--}3400\text{ cm}^{-1}$ correspond to the symmetric stretching vibration of OH from adsorbed H_2O on surface of as-synthesized Bi_2WO_6 and 5% $\text{Ag}_{0.9}\text{Pd}_{0.1}/\text{Bi}_2\text{WO}_6$ nanocomposites [14, 20].

Fig. 2b shows Raman spectra of as-synthesized Bi_2WO_6 and 5% $\text{Ag}_{0.9}\text{Pd}_{0.1}/\text{Bi}_2\text{WO}_6$ nanocomposites. The peaks in the wavelength range of $700\text{--}1000\text{ cm}^{-1}$ are assigned to W–O bond [2, 5, 14]. The asymmetric and symmetric A_g modes of terminal O–W–O vibration were detected at 792 and 843 cm^{-1} [2, 5, 14]. The shoulder Raman peak at 710 cm^{-1} is specified as asymmetric bridging in O–W–O chain [2, 5, 14]. The weak Raman peak at 402 cm^{-1} corresponds to the asymmetric mode of WO_6 octahedron [5]. The vibration of 300 and 310 cm^{-1} are assigned to the terminal WO_2 group and translational mode involving simultaneous motion of Bi^{3+} . The peak at 280 cm^{-1} corresponds to the bending mode of Bi–O bond [2, 5, 14].

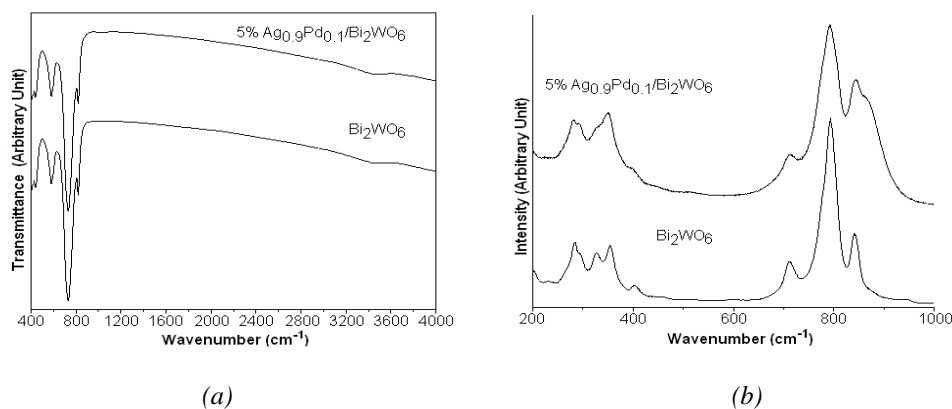


Fig. 2. (a) FTIR and (b) Raman spectra of Bi_2WO_6 and 5% $\text{Ag}_{0.9}\text{Pd}_{0.1}/\text{Bi}_2\text{WO}_6$ nanocomposites.

The morphology and microstructure of pure Bi_2WO_6 sample and 5% $\text{Ag}_{0.9}\text{Pd}_{0.1}/\text{Bi}_2\text{WO}_6$ nanocomposites were further examined by TEM. TEM image of pure Bi_2WO_6 sample as shown in Fig. 3a is composed of a number of thin nanoplates with average diameter of $50\text{--}80\text{ nm}$. Clearly, the surface of Bi_2WO_6 nanoplates is very smooth. The selected area electron diffraction (SAED) pattern of Bi_2WO_6 nanoplates is shown in Fig. 3b. The pattern can be indexed to the (113), (200), (202), (131) and (226) planes of orthorhombic Bi_2WO_6 structure. TEM image at low magnification of heterostructure 5% $\text{Ag}_{0.9}\text{Pd}_{0.1}/\text{Bi}_2\text{WO}_6$ nanocomposites (Fig. 3c) shows a number of sphere-like bimetallic AgPd nanoparticles embedded on top of Bi_2WO_6 thin nanoplates. A number of bimetallic spherical AgPd nanoparticles with $8\text{--}10\text{ nm}$ diameter are uniformly deposited on the surface of the Bi_2WO_6 nanoplates. The results indicate that the bimetallic AgPd nanoparticles were successfully loaded on the surface of Bi_2WO_6 nanoplates by photoreduction method and were promoted the effective separation of electrons and holes. The high resolution TEM (HRTEM) image of heterostructure 5% $\text{Ag}_{0.9}\text{Pd}_{0.1}/\text{Bi}_2\text{WO}_6$ nanocomposites (Fig. 3d) shows heterojunctions of bimetallic AgPd nanoparticles and Bi_2WO_6 thin nanoplates. The HRTEM image shows lattice fringes with spacing of 0.236 nm and 0.272 nm corresponding to the (111) plane of Ag (JCPDS no. 03-0921) and the (200) plane of Bi_2WO_6 . Thus, the nanocomposites improve the photocatalytic reaction by forming

Schottky barrier of AgPd/Bi₂WO₆ [1, 10, 12]. The results further certify that the surface of Bi₂WO₆ thin nanoplates was decorated by bimetallic AgPd nanoparticles by forming metal-semiconductor heterojunction.

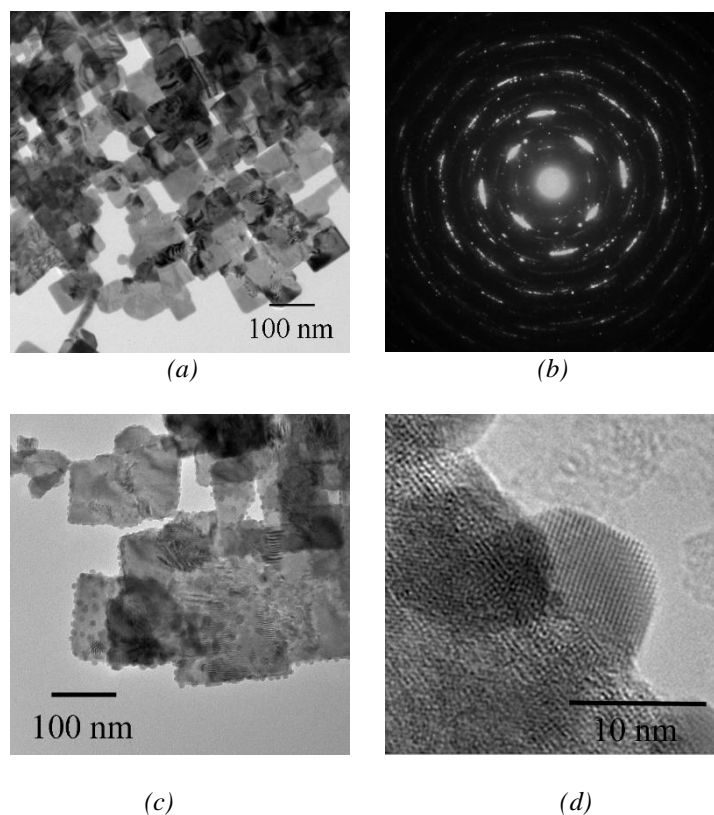


Fig. 3. TEM images, SAED pattern and HRTEM image of (a, b) Bi₂WO₆ and (c, d) 5% Ag_{0.9}Pd_{0.1}/Bi₂WO₆ nanocomposites.

The elemental composition and chemical state of the heterostructure 5% Ag_{0.9}Pd_{0.1}/Bi₂WO₆ nanocomposites were characterized by XPS as the results shown in Fig. 4. The high resolution binding energy peaks at 367.73 and 373.69 eV are ascribed to the Ag 3d_{5/2} and Ag 3d_{3/2} core levels, indicating that Ag species mainly exist as metallic Ag⁰ in the AgPd/Bi₂WO₆ nanocomposites [23, 24]. The high resolution binding energies of Pd shows the binding energies of Pd 3d_{5/2} at 335.29 eV and 335.99 eV for Pd⁰ and Pd²⁺ species; and Pd 3d_{3/2} at 340.61 eV and 341.35 eV for Pd⁰ and Pd²⁺ species [1, 12, 25]. Bi 4f_{5/2} and Bi 4f_{7/2} of Bi 4f core levels containing in Bi₂WO₆ lattice show two symmetric binding energies at 164.84 eV and 159.53 eV which are the characteristic of Bi³⁺ oxidation state [1, 2, 5, 6, 16]. The binding energies of W⁶⁺ oxidation state were detected at 37.95 eV of W 4f_{5/2} and 35.82 eV of W 4f_{7/2} with different spin-orbital of 2.13 eV [2, 5, 6, 16]. The high resolution binding energies of O 1s can be fitted to Gaussian peaks at 530.36, 531.16, 532.40 and 533.47 eV which are related to the Bi–O and W–O bonds of Bi₂WO₆ lattice and O–H bond of adsorbed H₂O and CO₂ on top of nanocomposites [1, 5, 6, 16].

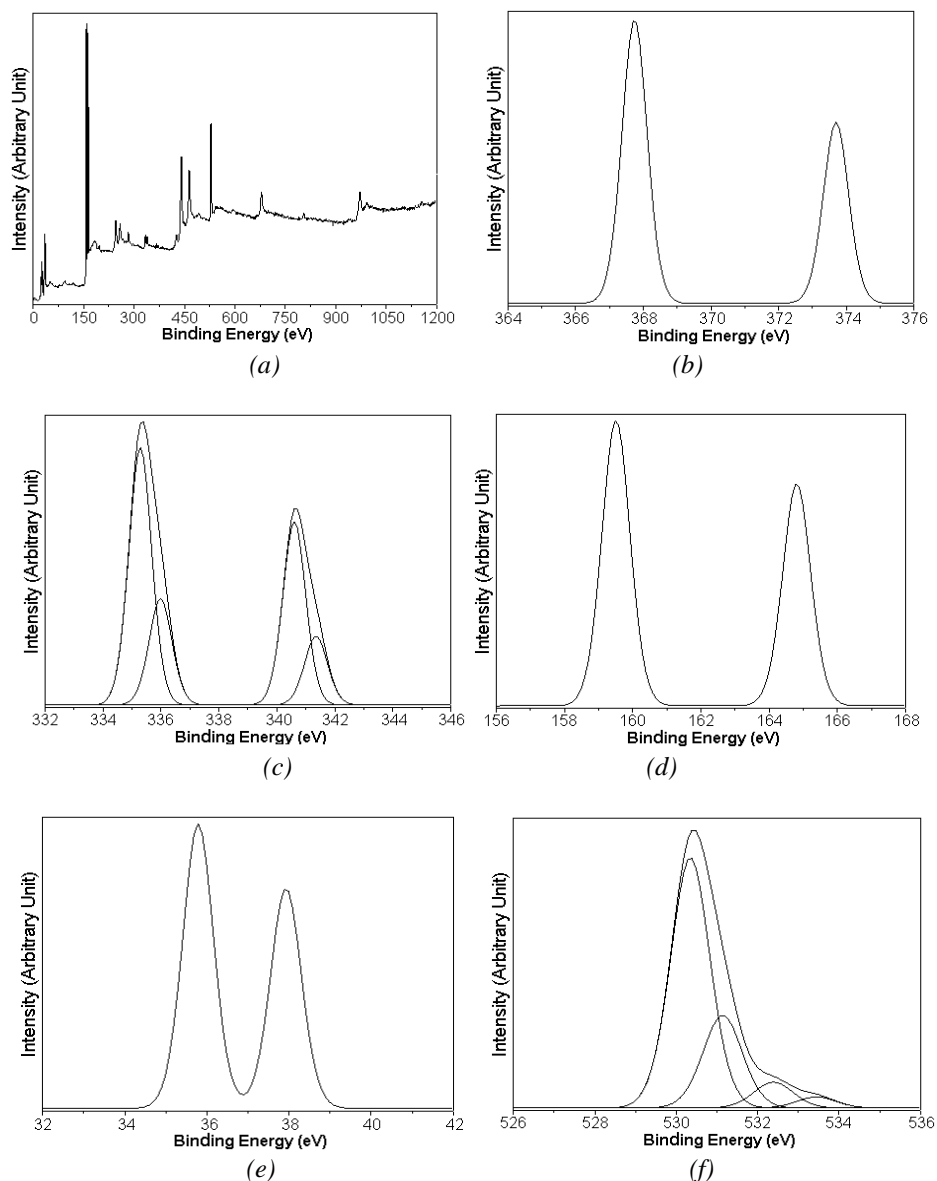


Fig. 4. (a) Full survey XPS spectrum and (b–f) high resolution XPS spectra of Ag 3d, Pd 3d, Bi 4f, W 4f and O 1s core levels of 5% $\text{Ag}_{0.9}\text{Pd}_{0.1}/\text{Bi}_2\text{WO}_6$ nanocomposites, respectively.

The photocatalytic performance of the prepared catalysts was evaluated for the degradation of RhB under visible-light irradiation. Fig. 5 shows the absorption spectra change in interval reaction time over heterostructure 5% $\text{Ag}_{0.9}\text{Pd}_{0.1}/\text{Bi}_2\text{WO}_6$ nanocomposites under visible light irradiation. It can be seen that the characteristic absorption peak of RhB solution gradually shifted from λ_{max} at 554 nm to 496 nm and the peak intensity was rapidly decreased to approach zero within 210 min. The maximum absorption in RhB was blue shifted because of the deethylation of ethyl groups in a stepwise manner [1, 3, 6, 15, 25]. It can be seen that the absorption of RhB in visible region over photocatalyst was decreased with the irradiation time increase. Thus, the aromatic ring of RhB molecule was also destroyed.

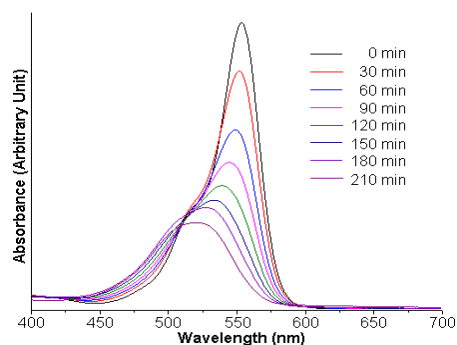


Fig. 5. UV-visible absorption for photodegradation of RhB in the presence of 5% $\text{Ag}_{0.9}\text{Pd}_{0.1}/\text{Bi}_2\text{WO}_6$ under visible light irradiation.

Fig. 6a shows photocatalytic efficiency of RhB degradation over as-synthesized Bi_2WO_6 and 5% $\text{Ag}_{0.9}\text{Pd}_{0.1}/\text{Bi}_2\text{WO}_6$ nanocomposites under visible light irradiation. Under visible light irradiation within 210 min, pure Bi_2WO_6 sample as photocatalyst exhibits rather poor photocatalytic efficiency towards RhB of 41.79% while heterostructure 5% $\text{Ag}_{0.9}\text{Pd}_{0.1}/\text{Bi}_2\text{WO}_6$ nanocomposites exhibits photocatalytic efficiency of 87.72%. Clearly, the photocatalytic performance of Bi_2WO_6 was enhanced after bimetallic AgPd nanoparticles were deposited on top. The pseudo-first-order linear relationship for photodegradation of RhB over as-synthesized Bi_2WO_6 and 5% $\text{Ag}_{0.9}\text{Pd}_{0.1}/\text{Bi}_2\text{WO}_6$ nanocomposites was revealed by the plot of $\ln(C_0/C_t)$ versus irradiation time (t) as the results shown in Fig. 6b. The photocatalytic rate constant of the samples was calculated [1, 6, 25]. The photocatalytic reaction rate constant for RhB degradation by as-synthesized Bi_2WO_6 and 5% $\text{Ag}_{0.9}\text{Pd}_{0.1}/\text{Bi}_2\text{WO}_6$ nanocomposites are $2.32 \times 10^{-3} \text{ min}^{-1}$ and $9.27 \times 10^{-3} \text{ min}^{-1}$. The photocatalytic reaction rate constant for heterostructure 5% $\text{Ag}_{0.9}\text{Pd}_{0.1}/\text{Bi}_2\text{WO}_6$ nanocomposites is much higher than that for pure Bi_2WO_6 because bimetallic AgPd nanoparticles as electron acceptor form an effective Schottky barrier with Bi_2WO_6 nanoplates which can lead to inhibit the recombination of electron-hole pair by transferring electron from conduction band of Bi_2WO_6 to bimetallic AgPd nanoparticles [1, 10, 12, 25, 26].

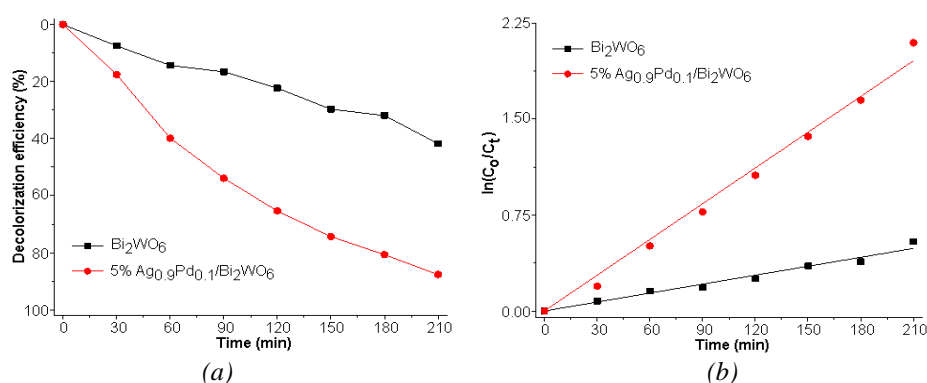


Fig. 6. (a) Decolorization efficiency and (b) first-order plot for photocatalytic degradation of RhB over Bi_2WO_6 and 5% $\text{Ag}_{0.9}\text{Pd}_{0.1}/\text{Bi}_2\text{WO}_6$ nanocomposites under visible light irradiation.

Fig. 7 shows a photocatalytic mechanism of heterostructure $\text{AgPd}/\text{Bi}_2\text{WO}_6$ nanocomposites under visible light irradiation. Under visible light irradiation, the photo-induced electrons and holes were generated in conduction band and valence band of Bi_2WO_6 [1, 8, 25, 26]. Then, the electrons in conduction band of Bi_2WO_6 migrate to the bimetallic AgPd nanoparticles through the Schottky barrier

which resulted in suppression of charge carrier recombination in the composites [1, 25, 26]. Moreover, the electrons on AgPd nanoparticles reacted with adsorbed O_2 as an oxidizing agent to form superoxide radical anions ($\bullet O_2^-$) as a reduced product. Concurrently, holes in valance band of Bi_2WO_6 reacted with adsorbed H_2O/OH^- as a reducing agent to form hydroxyl radical ($\bullet OH$) as oxidized product [1, 8, 25, 26]. They are extremely strong oxidant for degeneration of RhB to CO_2 and H_2O . The photocatalytic activity for heterostructure $AgPd/Bi_2WO_6$ nanocomposites was increased because bimetallic AgPd nanoparticles as electron acceptor can lead to suppress the recombination of photoinduced electrons and holes [1, 25, 26].

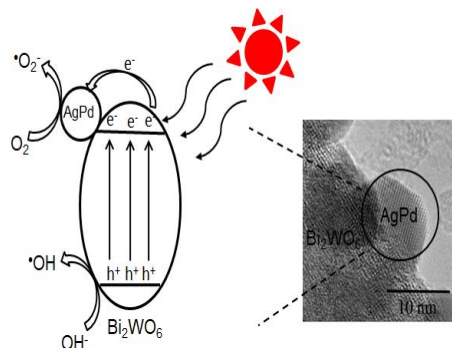


Fig. 7. Photocatalytic mechanism of heterostructure $Ag_{0.9}Pd_{0.1}/Bi_2WO_6$ nanocomposites under visible light irradiation.

4. Conclusions

In summary, 5% $Ag_{0.9}Pd_{0.1}/Bi_2WO_6$ nanocomposites were successfully synthesized by photoreduction deposition. The analytical results show good distribution of sphere-like bimetallic AgPd nanoparticles on the surface of orthorhombic Bi_2WO_6 thin nanoplates. The heterostructure 5% $Ag_{0.9}Pd_{0.1}/Bi_2WO_6$ nanocomposites show photodegradation of RhB better than pure Bi_2WO_6 nanoplates under visible light irradiation. This improvement is attributed to the migration efficiency of photoinduced carriers at the interface of 5% $Ag_{0.9}Pd_{0.1}/Bi_2WO_6$ nanocomposites.

Acknowledgements

The research was supported through the Faculty of Science Research Fund, Faculty of Science, Prince of Songkla University, Thailand, Contract no.1-2563-02-002.

References

- [1] A. Phuruangrat, T. Klangnoi, P. Patiphatpanya, P. Dumrongrojthanath, S. Thongtem, T. Thongtem, *J. Electron. Mater.* **49**, 3684 (2020).
- [2] L. Xiang, L. Chen, C. H. Mo, L. M. Zheng, Z. X. Yu, Y. W. Li, Q. Y. Cai, H. Li, W. D. Yang, D. M. Zhou, M.H. Wong, *J. Mater. Sci.* **53**, 7657 (2018).
- [3] Z. Zhu, Y. Yan, J. Li, *J. Mater. Sci.* **51**, 2112 (2016).
- [4] M. Darwish, A. Mohammadi, N. Assi, S. Abuzerr, Y. Alahmad, *Front. Chem. Sci. Eng.* **14**, 561020).
- [5] J. He, Q. Yu, Y. Zhou, Y. Wang, F. Long, *J. Wuhan Univ. Technol.-Mat. Sci. Edit.* **35**,

- 3482020).
- [6] S. Jonjana, A. Phuruangrat, N. Ekthammathat, S. Thongtem, T. Thongtem, *J. Electron. Mater.* **48**, 4789 (2019).
 - [7] X. Fan, X. Yue, J. Luo, C. Wang, *J. Nanopart. Res.* **18**, 65 (2016).
 - [8] S. Y. Wei, M. K. Li, D. Shang, N. Wang, L. X. Sun, Y. H. Xing, *J. Inorg. Organomet. Polym. Mater.* **25**, 1434 (2015).
 - [9] Y. Li, L. Cai, H. Wu, Q. Huang, Y. Du, S. Liu, Z. Sheng, C. Chen, *J. Wuhan Univ. Technol. Mat. Sci. Edit.* **34**, 1321 (2019).
 - [10] W. Xie, Z. Huang, R. Wang, C. Wen, Y. Zhou, *J. Mater. Sci.* **55**, 11829 (2020).
 - [11] J. Jiang, P. Zhao, L. Shi, X. Yue, Q. Qiu, T. Xie, D. Wang, Y. Lin, *J. Colloid Interf. Sci.* **518**, 102018.
 - [12] P. F. Lim, K. H. Leong, L. C. Sim, W. D. Oh, Y. H. Chin, P. Saravanan, C. Dai, *Appl. Phys. A* **126**, 550 (2020).
 - [13] Powder Diffract. File, JCPDS-ICDD, 12 Campus Bld., Newtown Square, PA 19073-3273, U.S.A. (2001).
 - [14] A. Phuruangrat, P. Dumrongrojthanath, N. Ekthammathat, S. Thongtem, T. Thongtem, *J. Nanomater.* **2014**, Art. ID. 138561 (2014).
 - [15] Y. Zhou, P. Lv, X. Meng, Y. Tang, P. Huang, X. Chen, X. Shen, X. Zeng, *Molecules* **22**, 859017).
 - [16] H. Shen, W. Xue, F. Fu, J. Sun, Y. Zhen, D. Wang, B. Shao, J. Tang, *Chem. Eur. J.* **24**, 18463 (2018).
 - [17] X. Tian, Z. Gao, F. Chen, Q. Wu, C. Li, W. Lu, Y. Sun, X. Tao, *CrystEngComm* **20**, 2669 (2018).
 - [18] A. Taoufyq, H. AitAhsaine, L. Patout, A. Benlhachemi, M. Ezahri, F. Guinneton, A. Lyoussi, G. Nolibe, J.R. Gavarri, *J. Solid State Chem.* **203**, 8 (2013).
 - [19] M. Maczka, L. Macalik, K. Hermanowicz, L. Kepínski, P. Tomaszewski, *J. Raman Spectrosc.* **41**, 1059 (2010).
 - [20] M. Zargazi, M. H. Entezari, *Ultrason. Sonochem.* **51**, 1 (2019).
 - [21] S. S. Lee, B. T. Huy, N. T. K. Phuong, D. K. Tung, Y. I. Lee, *Korean J. Chem. Eng.* **36**, 1716 (2019).
 - [22] F. He, Z. He, J. Xie, Y. Li, *Am. J. Anal. Chem.* **5**, 1142 (2014).
 - [23] M. Li, W. Huang, W. Qian, B. Liu, H. Lin, W. Li, L. Wan, C. Dong, *RSC Adv.* **7**, 46760 (2017).
 - [24] H. Y. Wu, W. J. Jian, H. F. Dang, X. F. Zhao, L. Z. Zhang, J. H. Li, *Pol. J. Environ. Stud.* **26**, 871017).
 - [25] A. Phuruangrat, T. Klangnoi, P. Patiphatpanya, P. Dumrongrojthanath, S. Thongtem, T. Thongtem, *Optik* **212**, 164674 (2020).
 - [26] A. Phuruangrat, P. Keereesaensuk, K. Karthik, P. Dumrongrojthanath, N. Ekthammathat, S. Thongtem, T. Thongtem, *J. Inorg. Organomet. Polymer. Mater.* **30**, 1033 (2020).